Ultrasound evaluation of the mechanical properties as an investigation tool for the wood-polymer composites including olive wood flour

Nesrine Bouhamed, Slim Souissi, Pierre Maréchal, Mohamed Ben Amar, Olivier Lenoir, Romain Léger, Anne Bergeret

HAL Id: hal-02765687

https://imt-mines-ales.hal.science/hal-02765687

Submitted on 16 Jun 2020

Ultrasound evaluation of the mechanical properties as an investigation tool for the wood-polymer composites including olive wood flour

Nesrine Bouhamed[a,b], Slim Souissi[a], Pierre Marechal[b,*], Mohamed Ben Amar[a], Olivier Lenoir[b], Romain Leger[c], Anne Bergeret[d]

[a] *Laboratory of Electromechanical Systems (LASEM), National Engineering School of Sfax, University of Sfax, 3038 Sfax, Tunisia*
[b] *Laboratoire Ondes et Milieux Complexes (LOMC), UMR CNRS 6294, 75 rue Bellot, Université Le Havre Normandie, 76600 Le Havre, France*
[c] *LMGC, IMT Mines Ales, Univ. Montpellier, CNRS, Ales*
[d] *Polymers Composites and Hybrids (PCH), IMT Mines Ales, Ales, France*

ABSTRACT

This paper presents results obtained for the development of a wood-polymer composite (WPC) based on polypropylene (PP) reinforced by olive wood fibers (OWF). The effect of the wood flour content and its chemical fiber treatment (amino-silane) on the mechanical properties of the WPC was studied by ultrasonic methods and mechanical tensile test. The elastic properties of the studied PP/OWF compositions are discussed and both of the mentioned evaluations give similar tendencies even if the characterization methods are somewhat different. As a result, the increase of the fiber content and the addition of the amino-silane coupling agent is shown to improve the rigidity of composite materials. Eventually, a correlation factor between the estimated Young's moduli is established between the ultrasound values (for $\varepsilon < 0.05\%$) and mechanical values (for $0.05 < \varepsilon < 0.25\%$). Ultrasound measurements are discussed as an alternative method for the elastic properties evaluation.

1. Introduction

The interest in fibers incorporated in polymers has been demonstrated for elastic properties improvement (Liang, 2012). The growing interest in the use of natural fibers (Oksman, 2000; Biagiotti et al., 2004; Puglia et al., 2005; Pickering et al., 2016; Dong, 2018; Mochane et al., 2019; Swolfs et al., 2019), lead to consider the olive wood fibers (OWF) of major ecological and economical interests. Indeed, among the fruit crops, olive is widely cultivated around the Mediterranean area. Tunisia is one of the first producers and exporters of olive oil in this region with more than 1.8 million hectares of olive trees cultivated in 2014 (Ben Mohamed et al., 2018). However, the oil extraction system generates a large volume of liquid and solid waste, which represents a potential problem of environmental pollution. Also, the olive wood used for the manufacture of handicraft products generates large quantities of waste composed of cellulose and lignin as the main elements (Gharbi et al., 2014; Naghmouchi et al., 2015). Furthermore, in parallel with glass and carbon fibers, various polymers have been investigated as possible matrices for natural fibers, due to their low cost, light weight, and high biodegradability (Amar et al., 2011; Djidjelli et al., 2007; Qiu and Netravali, 2012). Nevertheless, various classical polymers are always dominating the area of polymers for wood polymer composites (WPC). Among them, one can cite polyester, epoxies (Marrot et al., 2014), phenolics among the thermosets and polyethylene (PE) (Fortini and Mazzanti, 2018; Haddar et al., 2017; Santoni et al., 2018), polystyrene (PS), polyurethane (PU) (Tausif et al., 2017), polyvinyle chloride (PVC) and polypropylene (PP) (Bledzki et al., 2005; Bledzki et al., 2012; Bledzki et al., 2010; Stark, 2001; Dányádi et al., 2010; Nuñez et al., 2003) among the thermoplastics.

Indeed, the current study is carried out in the framework of biosourced materials. On the one hand, the studied WPC is based on a polymer matrix; on the other hand, wood filler particles are integrated as a load with the view to increasing the stiffness of the resulting composite material. This kind of WPC material raises questions about the methods of control and characterization either during manufacture or even after a period of service. Moreover, such a WPC material is expected to show viscoelastic properties, which can be highlighted by destructive mechanical tests and compared with a non-destructive ultrasound inspection. Non-destructive testing (NDT) may be a response to these questions thanks to the freedom of choice of sample geometry, the ability to obtain a high level of accuracy, quantity of information, speed and low cost of experiments. In fact, the applications of NDT methods for the mechanical characterization of materials are

---

increasingly numerous (Kundu, 2013). These methods are an alternative to the conventional destructive mechanical tests.

Among the non-destructive techniques, ultrasound characterization can be used to evaluate the elastic properties of the inspected samples. Lefebvre et al. (Lefebvre et al., 2018) used the Fabry-Pérot resonance technique to deduce the shear and bulk modulus of a viscoelastic polymer. El-Sabbagh et al. (El-Sabbagh et al., 2013) studied the effect of the natural fibers content on the ultrasound velocity in a composite material based on a polymer matrix. Ghodhbani et al. (Ghodhbani et al., 2015; Ghodhbani et al., 2016) used ultrasound to monitor the cure kinetics of an epoxy resin. Castellano et al. (Castellano et al., 2014) have performed the mechanical characterization of a bio-composite material by ultrasonic testing. Merotte et al. (Merotte et al., 2016) have controlled the porosity of a bio-composite by mechanical and acoustic methods. Castellano et al. (Castellano et al., 2016) used the ultrasonic wave immersion method to perform a mechanical characterization of a composite material.

The evaluation of longitudinal and transversal wave velocity is an efficient characterization method of an isotropic elastic material (Simonetti and Cawley, 2004; Simonetti et al., 2005; Afifi, 2003; Laperre et al., 1992), first for classifying the mechanical responses and then for determining the elastic moduli necessary for the description of the mechanical behavior (Scalerandi et al., 2012). The principle of this method is based on the time of flight measurement. This evaluation can also be performed in the spectral domain by Fourier transform. It is known that the longitudinal sound velocity is a function of the properties of the material that, in turn, is related to the fiber content and the adhesion quality (El-Sabbagh et al., 2013). As shown in previous studies, bio-composite materials constituted of a thermoplastic polymer as matrix and natural micro-fibers as reinforcement are interesting both in research (Garkhail et al., 2000; Arbelaiz et al., 2006) and industrial manufacturing. In this work, a WPC was elaborated and characterized by studying the longitudinal and transversal sound waves to obtain the Young's modulus and the Poisson's ratio. These results are compared with those obtained with destructive techniques. The tensile tests are showing a non-linear behavior of the stress-strain relationship as it was highlighted experimentally with PP based bio-composites by Merotte et al. (Merotte et al., 2018) and Tanguy et al. (Tanguy et al., 2018).

In section II, the constitutive raw materials and elaboration of the WPC are described. In section III, the characterization of the manufactured samples is presented involving both ultrasound and mechanical methods. In section IV, the measurement results are shown and compared for both methods, and differences are highlighted. In section V, a discussion is developed on the basis of the previously described results with the view to arguing the non-linear behavior of such a WPC. Finally, the main results of this work are summarized as a short list of analysis and perspectives.

2. Materials and samples

2.1. Elaboration of PP/OWF composite

The polypropylene (PP) used in this study is a standard homopolymer PP H9069 which was provided by Total Refining & Chemicals. According to ISO 1133, this polymer has a melt flow index of the order of 25 g/10 min (230°C, 2.16 kg). As defined by the ISO 527-1 and 2 (ISO 527-1, 2012, ISO 527-2, 2012), the tensile strength of this polymer is 32 MPa, the tensile modulus is 1.6 GPa. As stated by ISO 2039-2, the Rockwell hardness is 95. The olive wood fibers (OWF) comes from the region of Sfax in central Tunisia. It is recovered from wood waste generated during artisan work using a vacuum cleaner. It is then sieved and stored in plastic bags to protect it from moisture. Two types of OWF are used as reinforcing fillers, untreated (OWF) and treated with 3% the amino-silane coupling agent (OWFT). The procedure adopted for the filler treatments with 3-aminopropyltriethoxysilane is as follows: a solution (60/40, v/v) ethanol/water was prepared, then the pH was

adjusted between 4 and 4.5 by the addition of some drops of glacial acetic acid. Then, the 3-aminopropyltriethoxysilane (3% based on the OWF content) was added. The hydrolysis of the prepared solution was carried out for 2 h at ambient temperature. Finally, the OWF was added and the suspension was kept for 3 h at 70 °C to ensure the adsorption of the amino-silane onto the OWF particles. Then, to eliminate all the absorbed moisture and to avoid the formation of agglomerates, the OWF are pre-dried at 105°C for 24 h before extrusion. The PP polymer and the OWF fibers are mixed in a twin screw extruder (DSM Xplore Netherlands) twinned in parallel co-rotation with 3 heating zones. The rotational speed of the screw was set at 100 rpm and the output of the material is 200 g/h. The diameter of the screw is 10 mm. The extrusion temperature was varied and optimized to obtain an homogeneous mixture and to avoid the degradation of the OWF. Optimized extrusion conditions were set at 200 °C. Thus, the fabrication process can be decomposed in two steps: extrusion of granulates, and then injection of samples. First, the OWF and the PP polymer are manually mixed and placed in the extruder hopper. The composite material pass through the different zones and are extruded through the cylindrical matrix with a 1 mm diameter; after that, the extrudates are cooled at ambient temperature and cut with a few millimeters length; the resulting extruded granulates are dried during 24 h at 60 °C. Second, the dried granulates are molded using the Demag Plastic Group Extra 50-200 machine. The injection is carried out at a temperature of 180 °C and a pressure of 100 bar for all the WPC samples.

2.2. Samples

The studied bio-composite consists of polypropylene (PP) plates loaded with olive wood flour (OWF or F for simplicity's sake) which can be treated with the coupling agent (C) amino-silane. As a result, two families of WPC are obtained, i.e. PP/OWF and PP/OWFT with different mass loading rates of 0, 10, 20 or 30%. Thus, the PP/OWF composites are manufactured following the composition of the mixtures as shown in Table 1.

Two geometries are fabricated: tensile specimens and plates for the tensile tests and ultrasound measurements, respectively. More precisely, they are designed according to the ISO 5527-2 standard (ISO 527-2, 2012) (Fig. 1 (a)), and the plates are dimensioned for a 5 MHz broadband frequency range characterization, with fixed dimensions: thickness $d_p = 4$ mm, width $l = 100$ mm and length $L = 120$ mm (Fig. 1 (b)).

Fig. 2 shows plates made with increasing fiber content (0, 10, 20 and 30%). Even if some microscopic heterogeneities can be observed, those sample tensile test specimens and plates are considered homogeneous and isotropic and characterized as it.

3. Ultrasonic characterization

In this section, the ultrasound and mechanical measurements are presented and compared as possible characterization methods, each having its advantages and drawbacks. The obtained results are discussed and compared. On the one hand, for the ultrasonic measurements, the composite plate samples are immersed in a water tank only during the measurement which does not exceed 20 min in order to avoid the moisture content in the specimens. On the other hand, for the

Table 1
Experimental PP/OWF compositions as a function of the OWF charge load (F) and coupling agent (C).

Loaded PP	PP	10F/0C	20F/0C	30F/0C	7F/3C	17F/3C	27F/3C
PP	100	90	80	70	90	80	70
OWF	0	10	20	30	7	17	27
Amino-silane	0	0	0	0	3	3	3

(a)   (b)

Fig. 1. Injected samples made of PP/OWF for (a) Tensile tests according to the half-size ISO 527-2 and (b) Ultrasound characterization of plates designed for a 5 MHz broadband frequency range.

tensile test, the specimens are placed in a tensile test machine. These two methods are different but awaited to give comparable results.

3.1. Longitudinal wave measurement

The calculation of the propagation velocity of the wave in a material by flight time measurements is made from the first two echoes reflected by the walls of the plate. In this view, the configuration corresponding to a three-layer structure: water (index 1), the plate made of PP/OWF (index 2), water (index 3) is studied.

Fig. 3 illustrates the experimental device used. In Fig. 3 (a), the incident wave propagates at normal incidence relatively to the plate; it corresponds to the case of the measurement of longitudinal wave velocity c_L. In Fig. 3 (b), the incident wave propagates at oblique incidence θ relatively to the normal of the plate. More precisely, the transversal wave velocity c_T is measured for an incidence angle $\theta_L{}^c \leq \theta \leq \theta_T{}^c$, where $\theta_L{}^c$ and $\theta_T{}^c$ are the longitudinal and transversal critical angles, respectively.

3.1.1. Time of flight method

The pulse-echo method results in round-trip echoes $s_n(t)$ corresponding to the convolution of a pulse $g(t)$ with the round-trip function $p_n(t)$ in the thickness d_p of the plate.

$$s_n(t) = g(t)*p_n(t) = g(t)*\left(T_{12}R_{23}T_{21}.\left(R_{12}R_{23}.\ e^{-2\alpha_L d_p}\right)^n.\ \delta\left(t - n\frac{2d_p}{c_L}\right)\right)$$
(1)

where T_{ij} and R_{ij} are the transmission and reflection coefficients (Conoir, 1987) from medium indexed i to j, respectively, $\{i, j\} \in \{1, 2, 3\}$ and $\delta(t)$ is the Dirac function.

As a result, the longitudinal wave velocity c_L and attenuation α_L can be evaluated as:

$$\begin{cases} c_L = \dfrac{2d_p}{\text{tof}(s_2(t)) - \text{tof}(s_1(t))} \\ \alpha_L = \dfrac{1}{2d_p}\ln\left(\dfrac{\max(s_2(t))}{R_{12}R_{23}.\ \max(s_1(t))}\right) \end{cases}$$
(2)

where $\text{tof}(s_n(t))$ is the time-of-flight and $\max(s_n(t))$ is the maximum amplitude of the considered n^{th} echo denoted as $s_n(t)$. As illustrated by Fig. 4, the specular echo (first one) is located around 0.8 μs, and the second one resulting from a reflection on the rear face is located around 3.8 μs. The third one observed around 6.8 μs results from an additional roundtrip in the thickness of the plate.

3.1.2. Spectral method

The spectral method allows us to find the ultrasonic properties with the Fourier transform (FT) of the roundtrip echoes. More precisely, this method consists in analyzing $S(f) = \text{FT}\{s(t)\}$, where $s(t)$ is the signal containing the two first roundtrip echoes, $s_1(t)$ and $s_2(t)$. As described

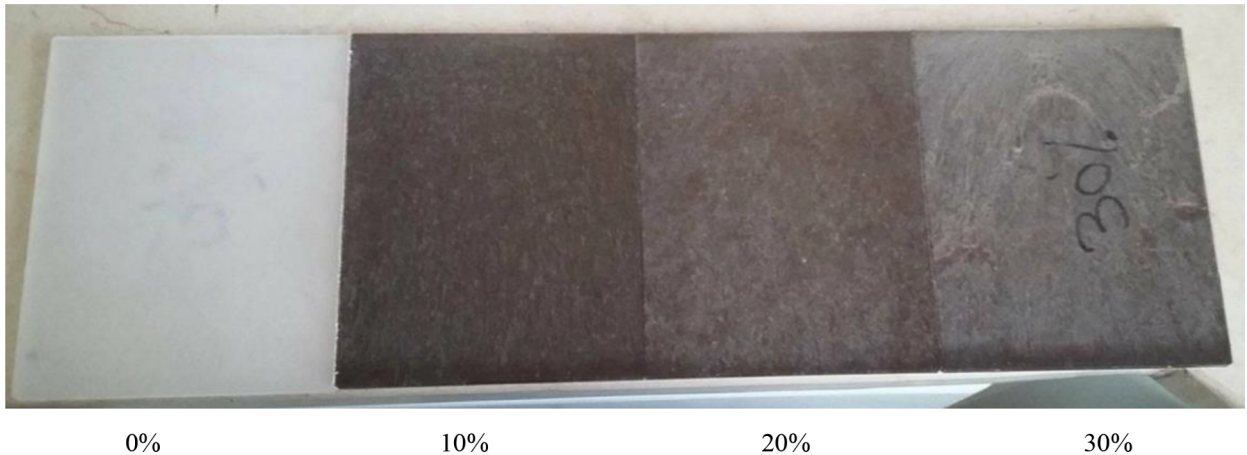0%   10%   20%   30%

Fig. 2. PP/OWF bio-composite plates with a mass fraction of OWF content of 0, 10, 20 and 30 %.
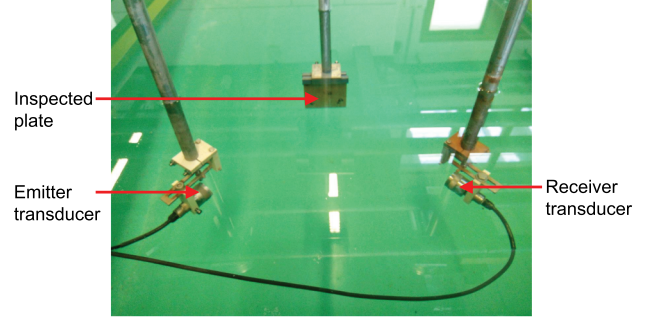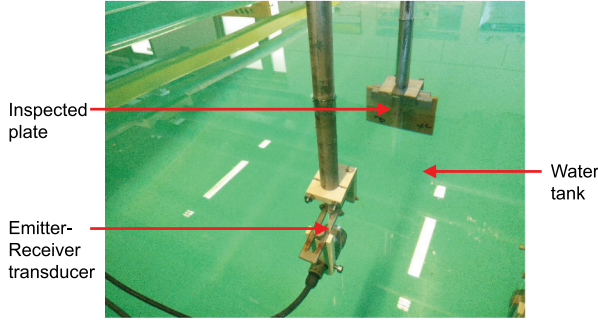
Fig. 3. Experimental setup for the measurements of (a) the longitudinal wave velocity, (b) the shear wave velocity.
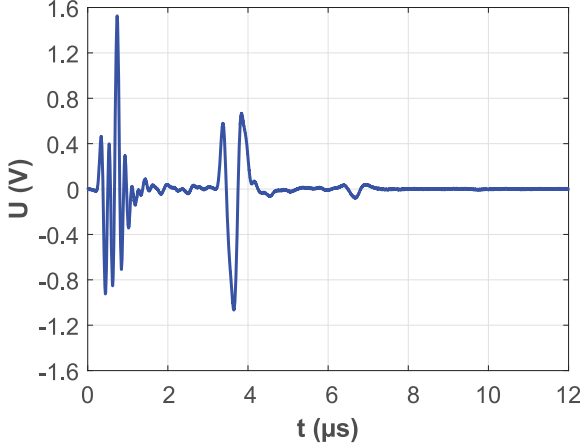

Fig. 4. Pulse-echo reflection at normal incidence on a PP/OWF (10%) plate.

by Eq. (3), these echoes are delayed by $\tau_L = 2d_p/c_L$ and this delay between the two echoes can be extracted from the calculated spectrum $\underline{S}(f)$:

$$s(t) = s_1(t) + s_2(t) = A_1 \cdot s_0(t - t_1) + A_2 \cdot s_0(t - t_2) \quad (3)$$

where $\begin{cases} A_2 = K \cdot A_1 \\ t_2 - t_1 = \tau_L \end{cases}$ and $\begin{cases} K = R_{12}R_{23} \cdot e^{-\alpha_L 2d_p} \\ \tau_L = \frac{2d_p}{c_L} \end{cases}$

The resulting FT gives:

$$\underline{S}(f) = \underline{S}_1(f) \cdot \underline{W}(f) = \underline{S}_1(f) \cdot \left(1 + K \cdot e^{+j2\pi f\tau_L}\right) \quad (4)$$

where $\underline{S}_1(f)$ is the spectrum of the signal $s_1(t)$, and $\underline{W}(f)$ is the weighting function.

Since $|K| \ll 1$, the modulus of this weighting function can be expanded as:

$$|\underline{W}(f)| \xrightarrow{K \ll 1} 1 + K \cos(2\pi f\tau_L) \quad (5)$$

As a result, the complex spectrum modulus $|\underline{S}(f)|$ (Fig. 5 (a)) exhibits regularly spaced minima with a frequency interval $\Delta f_L = 1/\tau_L = c_L/(2d_p)$. Thus, the longitudinal wave velocity c_L (Simonetti and Cawley, 2004) in the plate can be deduced from the following equation:

$$c_L = 2d_p \cdot \Delta f_L \quad (6)$$

3.2. Transversal wave measurement

For the measurements of the transversal velocity of the plates (Fig. 3 (b)), two transducers are used, one is the transmitter and the other one the receiver. The incident wave propagates in oblique incidence. The angle, referenced with respect to the normal of the plate, made by the beams generated or received by the two transducers is set according to the Snell-Descartes law. In this study, we have determined a longitudinal critical angle $\theta_L^c = 34°$ beyond which the longitudinal waves

do not propagate while the transversal waves still propagate. Therefore, the measurements are carried out with an angle of incidence $\theta = 40°$. We obtain a spectrum which exhibits regularly spaced minima with the frequency interval Δf_T (Fig. 5 (b)). As a result, in oblique incidence, beyond the longitudinal critical angle θ_L^c, the spectral method allows us to calculate the transversal propagation velocity c_T (Laperre et al., 1992) from the following equation:

$$c_T = \frac{2d_p \cdot \Delta f_T}{\sqrt{1 + \left(2d_p \cdot \Delta f_T \frac{\sin\theta}{c_w}\right)^2}} \quad (7)$$

where c_w is the sound speed in water with temperature compensation when needed (Bilaniuk and Wong, 1993).

3.3. Ultrasonic measurements

Using Eqs. (6) and (7), the spectral method is used to process the obtained echoes in order to evaluate the properties of the composite. As a result, the longitudinal wave velocity c_L (Fig. 5 (a)) and the transversal wave velocity c_T (Fig. 5 (b)) are deduced (Juliac et al., 1998; Waterman, 1963), respectively.

Fig. 6 (a) and (b) show the evolution of the longitudinal c_L and transversal c_T wave velocities as a function of the OWF reinforcement rate, respectively. These ultrasonic velocities c_L and c_T show an increasing trend. The higher the OWF rate, the more c_L and c_T increase. c_L from 2600 to 2750 m/s and c_T from 1272 to 1322 m/s, respectively. This ultrasonic shift relationship can be used to evaluate fiber homogeneity by taking multi-point measurements at different points in the sample (El-Sabbagh et al., 2013). Nevertheless, those measurement results are to be considered within a confidence interval, which was evaluated on the basis of an evaluation of the uncertainties. On the one hand, the uncertainty on the thickness of the plates was evaluated at 2% in the center of the plate. On the other hand, the measurements of frequency intervals Δf_L and Δf_T were evaluated to be constant in the bandwidth of the transducer within 2% and 6%, respectively. As a result, the global maximum uncertainty is illustrated with errorbars at $\Delta c_L/c_L \approx 4\%$ and $\Delta c_T/c_T \approx 8\%$ on the evaluated values of c_L and c_T, respectively. As shown in Fig. 6, the plots of the c_L and c_T wave velocities in the PP/OWFT bio-composite plates, made from OWF treated with the amino-silane, are greater than those of the PP/OWF plates, from raw OWF. This can be explained by the improvement of the WPC cohesion resulting from the treatment with the coupling agent that is amino-silane. Even if the addition of the coupling agent does not modify significantly the density (Table 2), the interest consists in increasing the cohesion between the two components: fibres and matrix. The direct effect is the increasing of the ultrasonic velocities c_L and c_T. In the following, it will be shown that this also leads to an increase of Young's modulus E_u.

The relationships between the ultrasound velocities (c_L, c_T) and the associated elastic properties (E_u, ν_u), i.e. Young's modulus and Poisson's ratio of the material for a homogeneous plate can be expressed as a
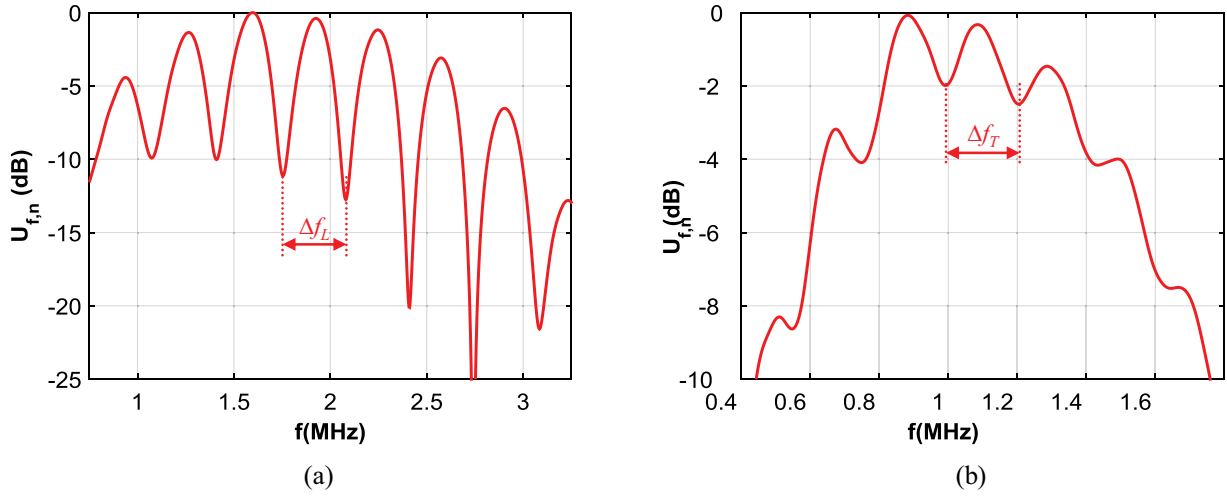
Fig. 5. Ultrasound wave velocity evaluation PP/OWF (10%): (a) at normal incidence for the longitudinal wave velocity c_L and (b) beyond the first critical angle for the transversal wave velocity c_T.

function of ρ the density, and the c_T/c_L ratio (Afifi, 2003; Benveniste and Milton, 2010):

$$
\begin{cases}
E_u = \rho c_T^2 \dfrac{3c_L^2 - 4c_T^2}{c_L^2 - c_T^2} = \rho c_L^2 \dfrac{3 - 4(c_T/c_L)^2}{1 - (c_T/c_L)^2}(c_T/c_L)^2 \\
\nu_u = \dfrac{1}{2} \dfrac{c_L^2 - 2c_T^2}{c_L^2 - c_T^2} = \dfrac{1}{2} \dfrac{1 - 2(c_T/c_L)^2}{1 - (c_T/c_L)^2}
\end{cases}
\tag{8}
$$

These parameters are known to have sensitive properties relatively to the fabrication process, particularly for polymer materials (Zihlif et al., 1982). This makes it possible to study the effect of the fiber content and the chemical treatment by the amino-silane on the elastic mechanical properties of composites indirectly by studying the velocities of the longitudinal and transversal waves. The densities of the samples can be calculated using the mixture rule given above, taking into account the treated and untreated fibers and knowing the densities of the various constituents:

$$
\rho_{th} = \left(\sum_i \frac{m_{f,i}}{\rho_i} \right)^{-1}
\tag{9}
$$

where $m_{f,i}$ is the mass fraction and ρ_i is the density, where $i \in \{reinforcement, matrix, load\}$.

As summarized in Table 2, these theoretical values ρ_{th} (Eq. (9)) were compared in very good agreement within 3% of relative error with those obtained experimentally ρ_{exp}.
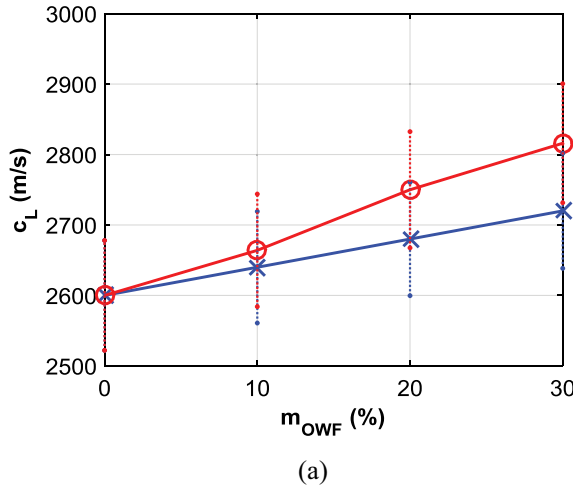
Table 2
Effect of the OWF charge load (F) and coupling agent (C) on density ρ and Poisson's coefficient ν_u.

Loaded PP	PP	10F/0C	20F/0C	30F/0C	7F/3C	17F/3C	27F/3C
ρ_{th} (kg/m³)	905	928	953	979	930	955	981
ρ_{exp} (kg/m³)	904	952	958	980	934	937	966
c_T/c_L	0.473	0.482	0.489	0.486	0.490	0.489	0.485
E_u (GPa)	3.71	4.05	4.40	4.61	4.25	4.64	4.93
ν_u	0.356	0.348	0.343	0.345	0.342	0.343	0.347

ρ_{th} (kg/m³): theoretical density; ρ_{exp} (kg/m³): experimental density; c_T/c_L: experimental transversal to longitudinal wave velocity ratio; (E_u, ν_u): experimentally deduced (Eq. (8)) Young's modulus and Poisson's ratio.

As a result, the ultrasound measurements (Fig. 6) allowed us to calculate the Poisson's coefficient ν_u (Eq. (8)) of the PP/OWF composite. This can be related to the ultrasonic velocities, density and mechanical properties (Gür, 2003) for a supposed homogeneous plate. One can observe that the variations of the Poisson's ratio ν_u as a function of the fiber content $m_{f,load}$ are not really significant (Fig. 7(b)). The measurements show that the wave velocity ratio is nearly constant $c_T/c_L \approx 0.48$, when the OWF charge load is within the range [0, 30%]. By expanding the expressions of (E_u, ν_u) (Eq. (8)) as a function of c_T/c_L in the vicinity of 1/2, we get:
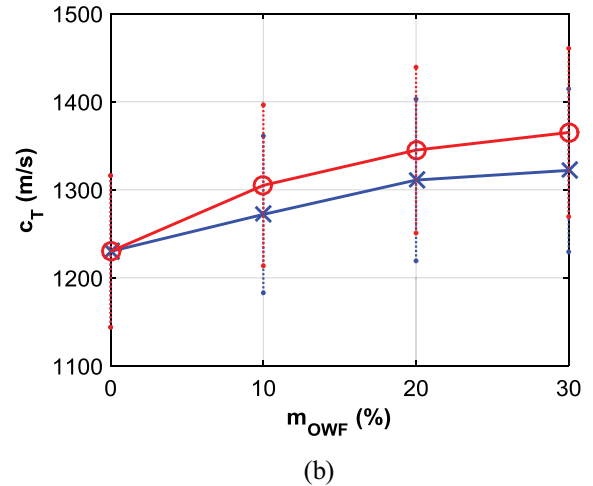

Fig. 6. Ultrasound wave velocity as a function of the OWF charge load (red circles for OWFT, blue cross for OWF): (a) longitudinal wave velocity c_L and (b) transversal wave velocity c_T. (For interpretation of the references to color in this figure legend, the reader is referred to the web version of this article.)
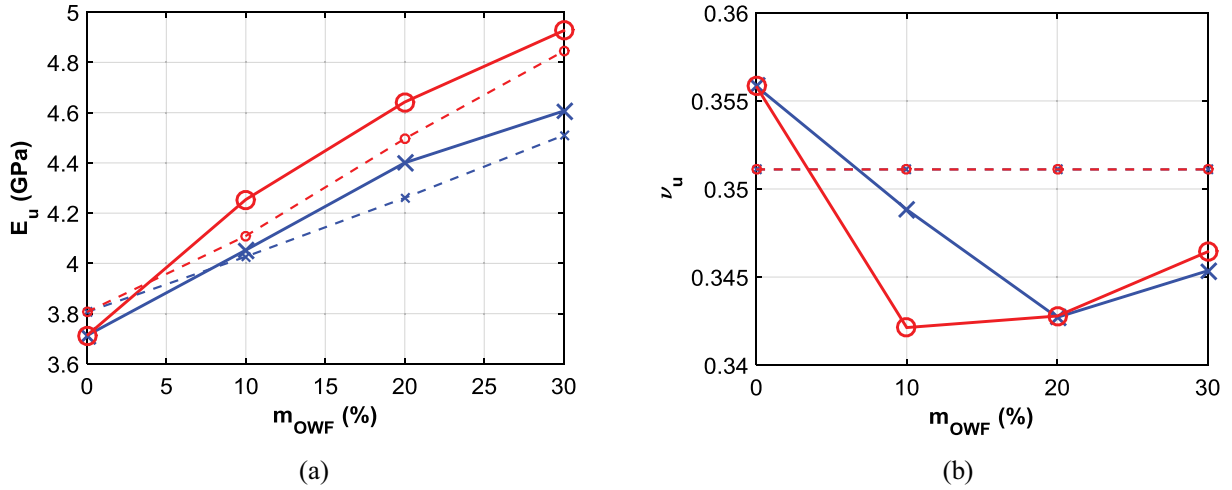
Fig. 7. Ultrasound measurements (solid line) and first order series expansion for $c_T/c_L \approx 0.48$ (dashed line) as a function of m_{OWF} (%) (red circles for OWFT, blue cross for OWF): (a) Young's modulus E_u and (b) Poisson's ratio ν_u. (For interpretation of the references to color in this figure legend, the reader is referred to the web version of this article.)

$$\begin{cases} E_{u,1} \approx \dfrac{2}{3}\rho c_L^2 \left(1 + \dfrac{10}{3}\left(\dfrac{c_T}{c_L} - \dfrac{1}{2}\right)\right) \\ \nu_{u,1} \approx \dfrac{1}{3}\left(1 - \dfrac{8}{3}\left(\dfrac{c_T}{c_L} - \dfrac{1}{2}\right)\right) \end{cases}$$

(10)

These correspondences between elastic mechanical and ultrasound variables (Eq. (8)) are valid in the strict sense for materials considered elastic, homogeneous and isotropic. In the present case, this assumption is to be verified. For the measurements, the used ultrasonic wavelength is $\lambda = c_L/f_0 = 2600/(5.10^6) \approx 520$ μm, to be compared to the OWF dimensions with an average size of 115 μm. Thus, the ratio between wavelength and OWF particles is of the order of 0.22, validating the long wavelength assumption. As a result, the effect of the quality of the fiber/matrix interface (cohesion) and the percentage of voids (porosity rate) are not observable by ultrasound, but are the actual result of an homogenization. The plot of the E_u ultrasound Young's modulus as a function of m_{OWF}, shows the stiffening effect of these fibers (Fig. 7). The experimental values of the ultrasound Young's modulus E_u (Fig. 7 (a)) show a nearly proportional increase with the OWF mass fraction, both for the treated and untreated plates. Indeed, the Young's modulus E_u increases from 3.7 GPa for the PP up to 4.6 GPa and 4.9 GPa for a 30% OWF and 30% OWFT charge loads, respectively.

4. Mechanical characterization

4.1. Tensile tests

As illustrated in Fig. 8, tensile tests are performed on a device (MTS Criterion) with a load cell of 1 kN. These tests are performed on half-size scale samples made in accordance with ISO 527-2 (ISO 527-2, 2012). The tensile test conditions are performed according to the ISO 527-1 (ISO 527-1, 2012), i.e. crosshead speed is set to 1 mm/min. In order to guarantee the reproducibility, five samples were successively placed between two supports and tested in the same experimental conditions. The strain measurement is obtained using a laser extensometer. As defined in the ISO 527-1, the Young's modulus is evaluated as the slope of the stress-strain curves between 0.05% and 0.25% of strain.

4.2. Mechanical measurements

By using the tensile test, the mechanical Young's modulus E_m is obtained (Fig. 9 (a)) and then compared to the ultrasound Young's

modulus E_u (Fig. 9 (b)). In this view, the ratio E_u/E_m between the ultrasound E_u and mechanical E_m moduli is plotted as a function of the OWF content m_{OWF}.

The experimental values of the mechanical Young's modulus E_m (Fig. 9 (a)) increase as a function of the OWF mass fraction, for both the treated and untreated plates. The rigidity of the plates increases with the addition of fibers and the treatment with the amino-silane. Nevertheless, as illustrated by Fig. 9 (b), even if the values are of the same order of magnitude, they are different. A correlation factor can be established in order to replace the mechanical destructive testing by the ultrasound non-destructive one. The ratio E_u/E_m decreases from 1.8 to 1.4. Fig. 10 shows that this difference is due to the definition of the Young's modulus E, which is commonly evaluated as the slope $[\partial\sigma/\partial\varepsilon]_{\varepsilon\to 0}$ at the origin of the tensile test curve $\sigma(\varepsilon)$ (Fig. 10 (a)). On the one hand, the Young's modulus in its mechanical definition E_m according to ISO 527-1 (ISO 527-1, 2012) is given by:

$$E_m = \frac{\sigma_2 - \sigma_1}{\varepsilon_2 - \varepsilon_1}$$

(11)

where $\{\sigma_1, \sigma_2\}$ are the measured stress values at normalized strain $\{\varepsilon_1 = 0.05\%; \varepsilon_2 = 0.25\%\}$, with a strain rate of $\partial\varepsilon/\partial t$ of 1 mm/min on a sample test of 58 mm long, i.e. $2.87.10^{-4}$ s^{-1}.

On the other hand, in the field of ultrasound E_u is evaluated in a range of strain before 0.05% (Fig. 10 (a)). Regarding the decrease of the slopes in the tensile curves (Fig. 10 (a)), the values of ultrasound evaluation E_u are systematically more important than the mechanical measurements E_m (Fig. 10 (b)).

As illustrated in Fig. 10 (a), the tensile curve $\sigma(\varepsilon)$ do not seem to show a linear behavior for small strain values, i.e. $\varepsilon < 0.5\%$. One can observe the classical evolution expected for a thermoplastic polymer, i.e. a non-linear behavior. The plot of the slope $\partial\sigma/\partial\varepsilon$ is also carried out and shown in Fig. 10 (b). It is observed that it is monotonously decreasing, whereas a constant step is expected in linear elasticity. More precisely, the slope $\partial\sigma/\partial\varepsilon$ curve exhibits a first rapid decrease in the range $\varepsilon \in [0\%, 0.05\%]$ and then it shows a moderate and constant decrease in the range $\varepsilon \in [0.1\%, 0.5\%]$. Thus, differences between ultrasonic and static stiffness measurements could be explained through the material viscoelastic properties: in ultrasound measurement, strain is small and strain rate is high while in static measurements strain is higher and strain rate is much lower. Even if this non-linear behavior has yet been highlighted (ISO 527-1, 2012, ISO 527-2, 2012, ASTM D638-03, 2003), especially for the thermoplastic polymer materials, a discussion on the subject is still to be developed. It is the object of the next section.
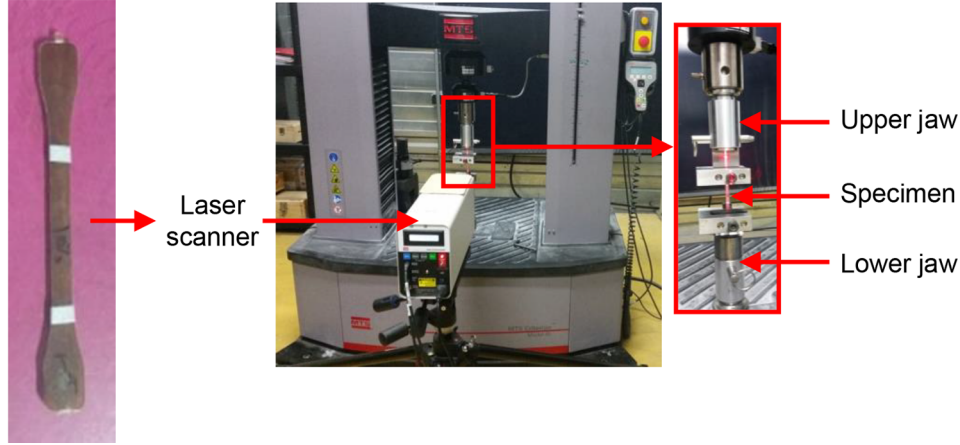
Fig. 8. Tensile test machine and associated laser scanner for the strain measurement.

5. Discussion

This tendency is observed whatever the OWF or OWFT mass fraction m_{OWF} in the samples, from 0 to 30%. As a result, the tensile curve $\sigma(\varepsilon)$ (Fig. 11 (a)) shows a non-linear increase, and additionally, the slope $\partial\sigma/\partial\varepsilon$ (Fig. 11 (b)) also shows non-linear decreasing. This non-linear behavior of polymers is well-known and can be related to viscoelastic models of the stress-strain function $\sigma(\varepsilon)$ (Khan et al., 2012; Kolarík and Pegoretti, 2006). It can also be argued that the PP/OWF composite is not homogeneous and the fibers are not uniformly dispersed in the PP matrix (Martin et al., 2013). As a consequence, viscoelasticity lead to reconsider the standard elastic stress-strain function involving the Young's modulus E with a frequency and temperature dependence (Madigosky and Lee, 1983; Lagakos et al., 1986; Guillot and Trivett, 2003). Particularly, the frequency and temperature dependence of the Young's modulus has been evaluated in polypropylene 6823 (Lagakos et al., 1986). Also, due to viscoelasticity, the strain velocity $\partial\varepsilon/\partial t$ as well as temperature T are key parameters for the evaluation of the Young's modulus E. This has been experimentally demonstrated, modeled and discussed by Mulliken and Boyce (Mulliken and Boyce, 2006), Siviour and Jordan (Siviour and Jordan, 2016) and Cho et al. (Cho et al., 2017). Indeed, special attention was paid in this study to keep constant the strain velocity $\partial\varepsilon/\partial t$ and temperature T so that

their influence can be considered as fixed.

In the case of materials of the family of polymers, the elastic properties are very sensitive to the considered deformation zone [ε_{min}, ε_{max}], to the scale effects (size of the specimens) and very dependent on the strain velocity $\partial\varepsilon/\partial t$ and temperature T (Schiavi and Prato, 2017; Johnson and Cook, 1983).

A first approach lead us to consider that the non-linear behavior of the tensile curve $\sigma(\varepsilon)$ can be fitted by a power law, where the power factor is inferior to one. It is called the Hollomon's law given by:

$$\sigma = K \cdot \varepsilon^n \tag{12}$$

Using this power law, the experimental data are fitted with such a relation (Fig. 12 (a)). The Hollomon's law resulting from the set of the two parameters (K, n) is illustrated in Fig. 12 (b) by the plot of the tensile curves, including the strain range $\varepsilon \in [0.05\%, 0.25\%]$ corresponding to ISO 527-2.

The linear regression of the log-log plots in the strain range $\varepsilon \in [0.05\%, 0.25\%]$ (Fig. 12 (a)) allows us to obtain the two unknown parameters, i.e. the intercept corresponding to the logarithmic value of the rigidity K (Fig. 13 (a)) and the slope corresponding to the power law parameter n (Fig. 13 (b)). The rigidity K varies from 0.29 to 0.55 GPa, and the power law parameter n is between 0.63 and 0.67.

A fit of the Hollomon's law around a reference point $\varepsilon_{ref} = 0.15\%$ leads to relate an evaluated reference Young's modulus E_{ref} (Fig. 13 (c))
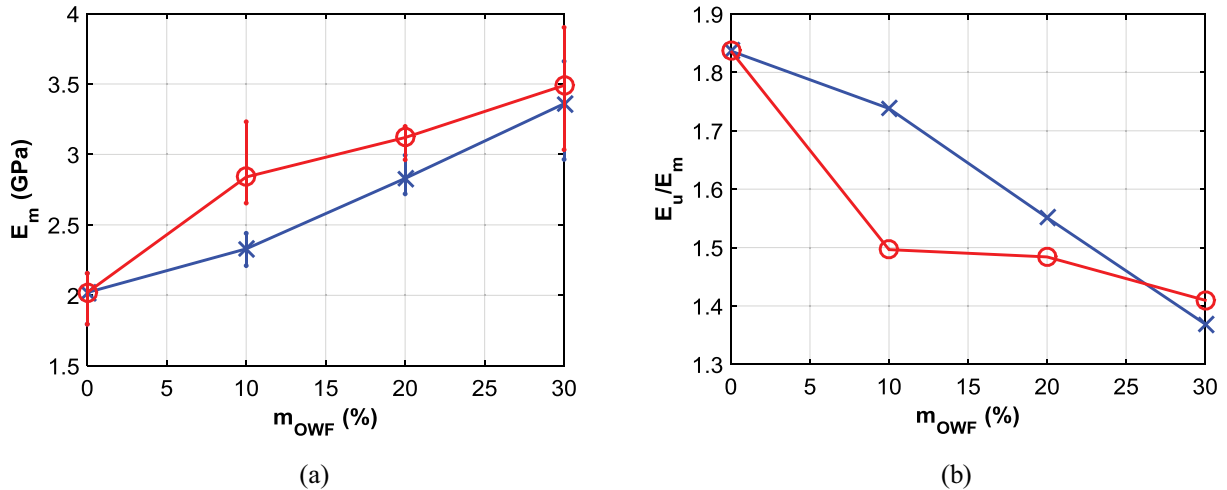

(a)

(b)

Fig. 9. Young's modulus (a) E_m evaluated by tensile test and (b) E_u/E_m ultrasound versus mechanical ratio as a function of m_{OWF} (%) (red circles for OWFT, blue cross for OWF). (For interpretation of the references to color in this figure legend, the reader is referred to the web version of this article.)
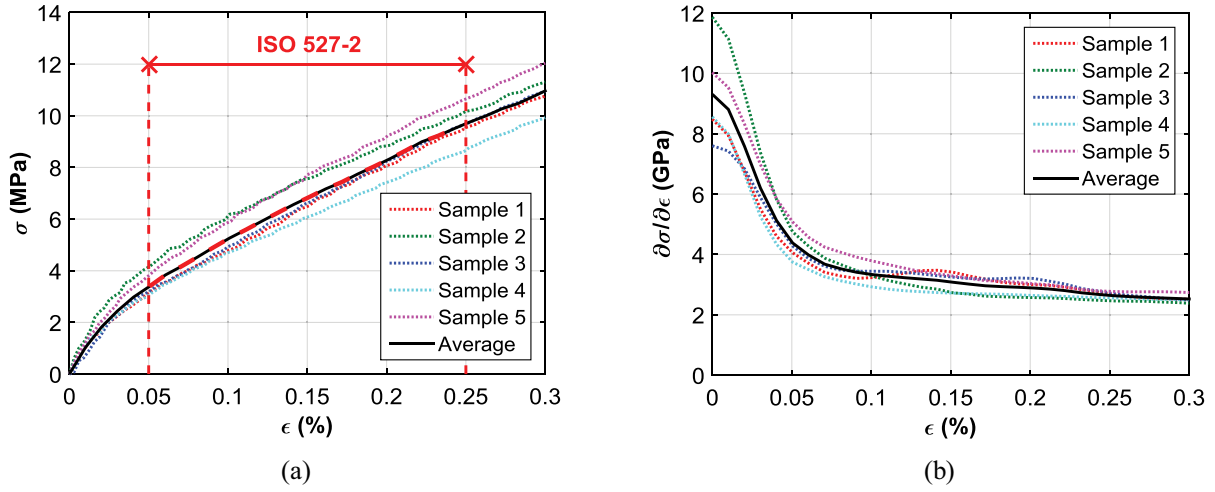
Fig. 10. Mechanical tensile test results on a PP/OWF at 30% WPC (a) $\sigma(\varepsilon)$ for ε ranging from 0 to 0.3% and (b) associated slope $\partial\sigma/\partial\varepsilon$ for ε ranging from 0 to 0.3%.

to the Hollomon's law parameters (K_{ref}, n_{ref}). Indeed, E_{ref} is defined by the following equation:

$$E_{ref} = \left[\frac{\partial\sigma}{\partial\varepsilon}\right]_{\varepsilon_{ref}} = K_{ref} . n_{ref} . (\varepsilon_{ref})^{n_{ref}-1} \tag{13}$$

From these results, one can observe that the power parameter n_{ref} is around $2/3 \pm 5\%$ and therefore, the effective reference elastic modulus E_{ref} can be approximated by:

$$E_{ref} \approx \frac{2}{3} K_{ref} . (\varepsilon_{ref})^{-\frac{1}{3}} \tag{14}$$

As a consequence, the elastic modulus E is a decreasing function of the strain ε. The obtained values for the elastic modulus parameter E_{ref} varying from 1.7 to 3.3 GPa are nearly the same as those obtained from classical Young's modulus evaluation E_m, from 2 to 3.5 GPa, under-estimating those obtained from ultrasound measurements E_u, from 3.7 to 4.9 GPa.

6. Conclusion

In this study, the influence of the content of natural fiber (OWF) in a thermoplastic matrix (PP) and the effect of chemical fiber treatment (addition of amino-silane coupling agent) is investigated. It is correlated to the Young's modulus of the WPC. Two types of tests have been carried out: on the one hand, a non-destructive evaluation using

ultrasound; on the other hand, a conventional destructive mechanical test, following the procedure described in the ISO 527-1 for the tensile test standard for polymers. The WPC are studied as a function of the m_{OWF} ratio from 0 to 30%, without coupling agent (PP/OWF) or with the adjunction of 3% of coupling agent (PP/OWFT).

The elastic properties of the studied PP/OWF compositions are discussed and both non-destructive and destructive evaluations give similar tendencies even if the measured values are somewhat different. The results can be summarized as follows:

– The increase of the fiber content and the addition of a coupling agent improves the rigidity of WPC;
– The rigidity is quantified and compared through the evaluation of the Young's modulus, either by the ultrasonic method or by the classical mechanical tensile test;
– A correlation factor between the estimated Young's moduli is established between the ultrasound values (for $\varepsilon < 0.05\%$) and mechanical values (for $0.05 < \varepsilon < 0.25\%$);
– The ultrasound measurements show that the longitudinal and transversal velocities increase in the same proportions, firstly with the fiber content and secondly with the addition of a coupling agent.

It is shown that in the case of the mechanical tests, the stress σ versus the strain ε curve is non-linear. The studied WPC are thermoplastic polymers and are known to have non-linear properties. More
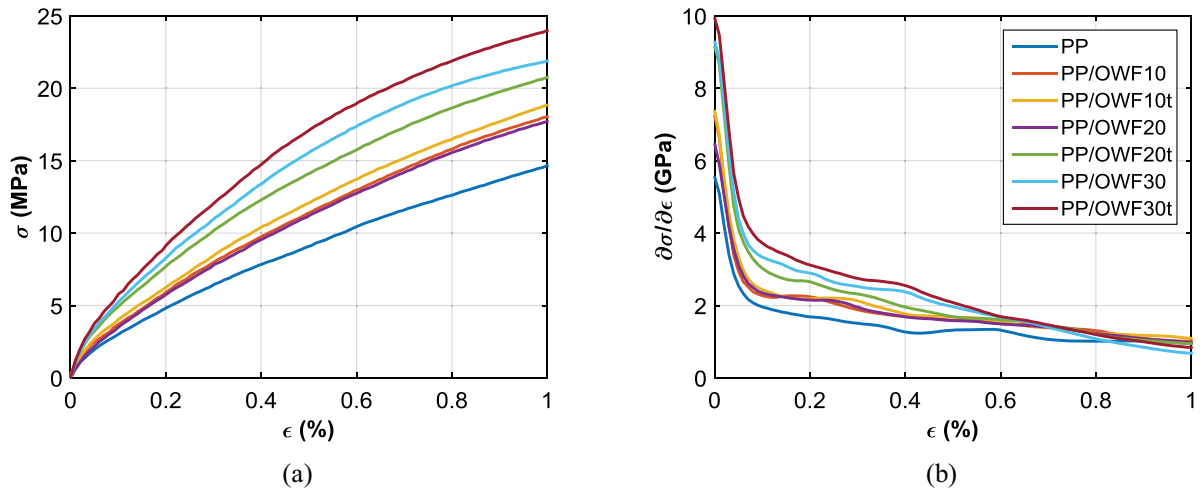

Fig. 11. Sensitivity of the WPC composition on (a) the stress σ and (b) the stress to strain slope $\partial\sigma/\partial\varepsilon$, as a function of the strain ε.
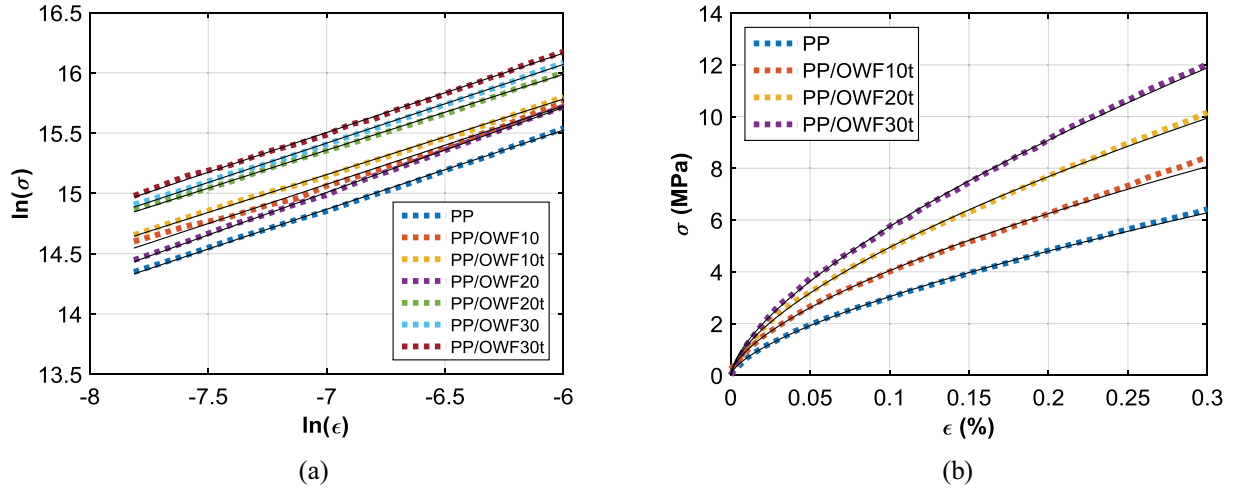
Fig. 12. (a) Log-Log plots of the stress σ versus the strain ε. (b) Plots of the stress σ versus the strain ε and associated Hollomon's fits (solid black).

precisely, these curves are fitted accurately with the Hollomon's power law in a large strain range. In order to compare the classical linear elastic properties, we evaluated the Young's modulus following the ISO 527-1 in a standard strain range. This standard states that the Young's modulus is evaluated by average slope of the tensile curve $\sigma(\varepsilon)$ in the

reference range 0.05 to 0.25%. An identification of the Hollomon's law parameters (K_{ref}, n_{ref}) and the estimated Young's modulus E_{ref} is performed, and it shows a good agreement.

This study highlights important differences due to the considered deformation domain of interest but confirms the order of magnitude. It
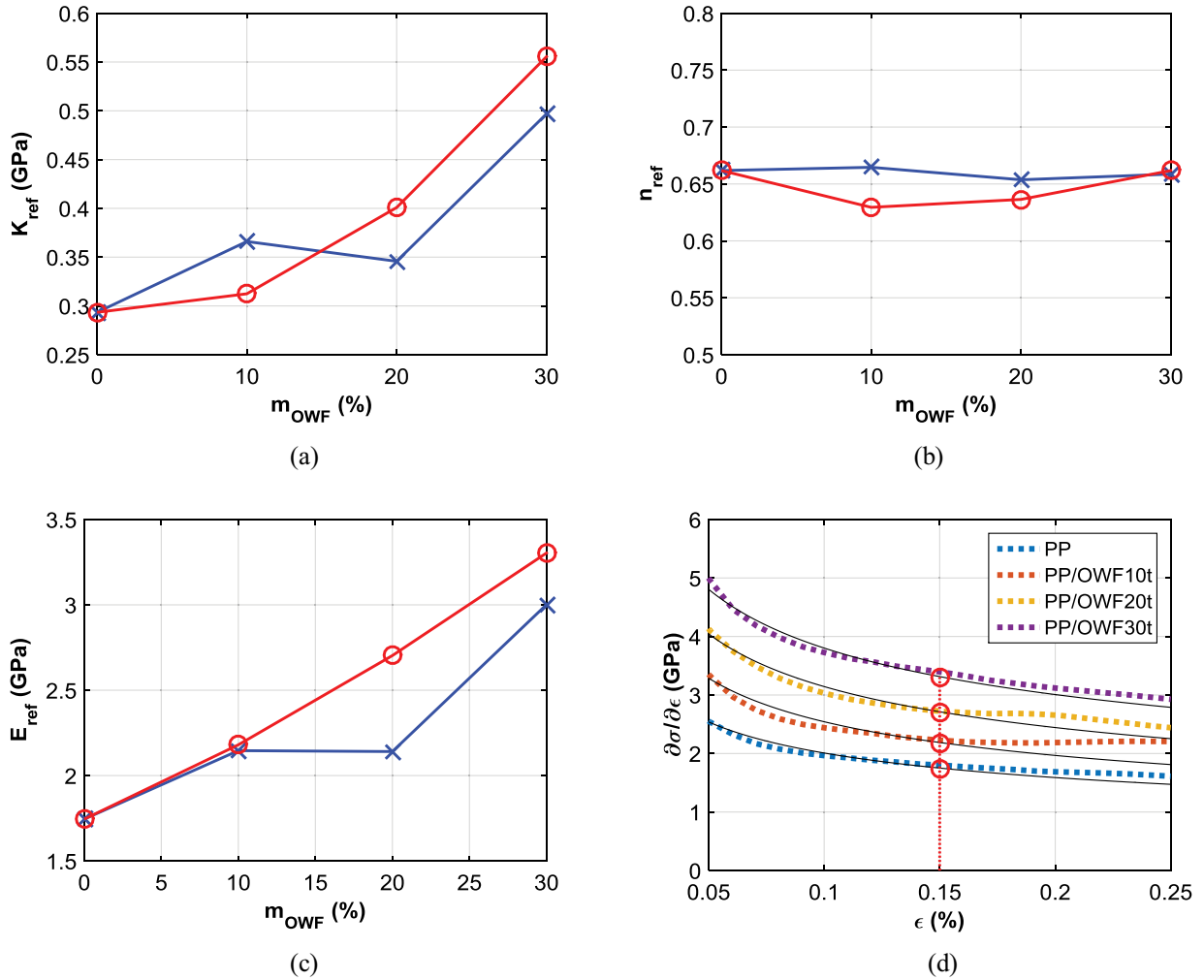

Fig. 13. Hollomon's parameters fitted in the strain range $\varepsilon \in [0.05\%, 0.25\%]$ as a function of m_{OWF} (%) (red circles for OWFT, blue cross for OWF): (a) K_{ref}, (b) n_{ref} (c) corresponding E_{ref} elastic modulus, (d) $\partial\sigma/\partial\varepsilon$ for OWFT, associated Hollomon's fits (solid black) and identified E_{ref} elastic modulus (red circles). (For interpretation of the references to color in this figure legend, the reader is referred to the web version of this article.)

also establishes a correlation factor between ultrasound and conventional tensile tests.

As a perspective, these first experimental results have to be consolidated with much more samples and tests. Among the possible experiments, many parameters of influence needs to be investigated such as strain velocity $\partial\varepsilon/\partial t$ and temperature T. Additional ultrasound experiments can be envisaged with contact transducers to confirm the values of the velocities and their homogeneity in the plate. Alternative characterization methods can be investigated such as flexural tests in the low frequency range.

Data availability

The raw/processed data required to reproduce these findings cannot be shared at this time due to technical or time limitations.

Supplementary materials

Supplementary material associated with this article can be found, in the online version, at doi:10.1016/j.mechmat.2020.103445.

References

Afifi, H.A., 2003. Ultrasonic pulse echo studies of the physical properties of PMMA, PS, and PVC. Polym.-Plast. Technol. Eng. 42 (2), 193–205. [Online]. Available: https://doi.org/10.1081/PPT-120017922.

Amar, B., Salem, K., Hocine, D., Chadia, I., Juan, M.J., 2011. Study and characterization of composites materials based on polypropylene loaded with olive husk flour. J. Appl. Polym. Sci. 122 (2), 1382–1394. [Online]. Available: http://dx.doi.org/10.1002/app.34084.

ASTM D638-03, 2003. ASTM D638-03 Standard Test Method for Tensile Properties of Plastics. American Society for Testing and Materials Std.. www.astm.org [Online]. Available: https://www.astm.org/DATABASE.CART/HISTORICAL/D638-03.htm.

Arbelaiz, A., Fernández, B., Valea, A., Mondragon, I., 2006. Mechanical properties of short flax fibre bundle/poly(ε-caprollate) composites: Influence of matrix modification and fibre content. Carbohydr. Polym. 64 (2), 224–232. [Online]. Available: http://www.sciencedirect.com/science/article/pii/S0144861705005801.

Ben Mohamed, M., Guasmi, F., Ben Ali, S., Radhouani, F., Faghim, J., Triki, T., Kammoun, N.G., Baffi, C., Lucini, L., Benincasa, C., 2018. The LC-MS/MS characterization of phenolic compounds in leaves allows classifying olive cultivars grown in South Tunisia. Biochem. Syst. Ecol. 78, 84–90. [Online]. Available: http://www.sciencedirect.com/science/article/pii/S0305197818301443.

Benveniste, Y., Milton, G., 2010. The effective medium and the average field approximations vis-à-vis the Hashin-Shtrikman bounds. I. The self-consistent scheme in matrix-based composites. J. Mech. Phys. Solids 58 (7), 1026–1038. [Online]. Available: http://www.sciencedirect.com/science/article/pii/S0022509610000839.

Biagiotti, J., Puglia, D., Kenny, J.M., 2004. A review on natural fibre-based composites - Part I. J. Nat. Fibers 1 (2), 37–68. [Online]. Available: https://doi.org/10.1300/J395v01n02_04.

Bilaniuk, N., Wong, G.S.K., 1993. Speed of sound in pure water as a function of temperature. J. Acoust. Soc. Am. 93 (3), 1609–1612. [Online]. Available: https://doi.org/10.1121/1.406819.

Bledzki, A., Letman, M., Viksne, A., Rence, L., 2005. A comparison of compounding processes and wood type for wood fibre-PP composites. Compos. Part A 36 (6), 789–797. [Online]. Available: http://www.sciencedirect.com/science/article/pii/S1359835X04002659.

Bledzki, A., Mamun, A., Bonnia, N., Ahmad, S., 2012. Basic properties of grain by-products and their viability in polypropylene composites. Ind. Crops Prod. 37 (1), 427–434. [Online]. Available: http://www.sciencedirect.com/science/article/pii/S0926669011001440.

Bledzki, A., Mamun, A., Volk, J., 2010. Physical, chemical and surface properties of wheat husk, rye husk and soft wood and their polypropylene composites. Compos. Part A 41 (4), 480–488. [Online]. Available: http://www.sciencedirect.com/science/article/pii/S1359835X09003972.

Castellano, A., Foti, P., Fraddosio, A., Marzano, S., Piccioni, M.D., 2014. Mechanical characterization of CFRP composites by ultrasonic immersion tests: Experimental and numerical approaches. Compos. Part B 66 (Supplement C), 299–310. [Online]. Available: http://www.sciencedirect.com/science/article/pii/S1359836814001802.

Castellano, A., Foti, P., Fraddosio, A., Marzano, S., Piccioni, M.D., 2016. A new ultrasonic immersion technique for the evaluation of damage induced anisotropy in composite materials. In: 3rd International Balkans Conference on Challenges of Civil Engineering, 3-BCCCE, 19-21 May 2016. Tirana, Albania. 66. Epoka University, pp. 273–282. [Online]. Available: http://www.sciencedirect.com/science/article/pii/S1359836814001802.

Cho, H., Mayer, S., Pöselt, E., Susoff, M., in't Veld, P.J., Rutledge, G.C., Boyce, M.C., 2017. Deformation mechanisms of thermoplastic elastomers: Stress-strain behavior and constitutive modeling. Polymer 128, 87–99. [Online]. Available: http://www.sciencedirect.com/science/article/pii/S0032386117308595.

Conoir, J., 1987. In: CEDOCAR, P., Gespa, N. (Eds.), Chap.5.

Dányádi, L., Móczó, J., Pukánszky, B., 2010. Effect of various surface modifications of wood flour on the properties of PP/wood composites. Compos. Part A 41 (2), 199–206. [Online]. Available: http://www.sciencedirect.com/science/article/pii/S1359835X09003285.

Djidjelli, H., Benachour, D., Boukerrou, A., Zefouni, O., Martinez-Vega, J., Farenc, J., Kaci, M., 2007. Thermal, dielectric and mechanical study of poly(vinyl chloride)/olive pomace composites. Exp. Polym. Lett. 1 (12), 846–852. [Online]. Available: http://www.expresspolymlett.com/letolt.php?file=EPL-0000470&mi=c.

Dong, C., 2018. Review of natural fibre-reinforced hybrid composites. J. Reinf. Plast. Compos. 37 (5), 331–348. [Online]. Available: https://doi.org/10.1177/0731684417745368.

El-Sabbagh, A., Steuernagel, L., Ziegmann, G., 2013. Ultrasonic testing of natural fibre polymer composites: effect of fibre content, humidity, stress on sound speed and comparison to glass fibre polymer composites. Polym. Bull. 70 (2), 371–390. [Online]. Available: https://doi.org/10.1007/s00289-012-0797-8.

El-Sabbagh, A., Steuernagel, L., Ziegmann, G., 2013. Characterisation of flax polypropylene composites using ultrasonic longitudinal sound wave technique. Compos. Part B 45 (1), 1164–1172. [Online]. Available: http://www.sciencedirect.com/science/article/pii/S1359836812003939.

Fortini, A., Mazzanti, V., 2018. Combined effect of water uptake and temperature on wood polymer composites. J. Appl. Polym. Sci. 135 (35), 46674. [Online]. Available: https://onlinelibrary.wiley.com/doi/abs/10.1002/app.46674.

Garkhail, S.K., Heijenrath, R.W.H., Peijs, T., Nov 2000. Mechanical properties of natural-fibre-mat-reinforced thermoplastics based on flax fibres and polypropylene. Appl. Compos. Mater. 7 (5), 351–372. [Online]. Available: https://doi.org/10.1023/A:1026590124038.

Gharbi, A., Bel Hassen, R., Boufi, S., 2014. Composite materials from unsaturated polyester resin and olive nuts residue: The effect of silane treatment. Ind. Crops Prod. 62, 491–498. [Online]. Available: http://www.sciencedirect.com/science/article/pii/S0926669014005573.

Ghodhbani, N., Maréchal, P., Duflo, H., 2015. Curing and post-curing viscoelastic monitoring of an epoxy resin. Phys. Procedia 70, 106–109. [Online]. Available: http://www.sciencedirect.com/science/article/pii/S1875389215007944.

Ghodhbani, N., Maréchal, P., Duflo, H., 2016. Ultrasound monitoring of the cure kinetics of an epoxy resin: identification, frequency and temperature dependence. Polym. Test. 56, 156–166. http://www.sciencedirect.com/science/article/pii/S0142941815302105.

Gür, C., 2003. Investigation of microstructure-ultrasonic velocity relationship in SiCp-reinforced aluminium metal matrix composites. Mater. Sci. Eng. 361 (1), 29–35. [Online]. Available: http://www.sciencedirect.com/science/article/pii/S0921509303005689.

Guillot, F.M., Trivett, D.H., 2003. A dynamic Young's modulus measurement system for highly compliant polymers. J. Acoust. Soc. Am. 114 (3), 1334–1345. [Online]. Available: https://doi.org/10.1121/1.1604121.

Haddar, M., Elloumi, A., Koubaa, A., Bradai, C., Migneault, S., Elhalouani, F., Sep 2017. Effect of high content of deinking paper sludge (DPS) on the reinforcement of HDPE. J. Polym. Environ. 25 (3), 617–627. [Online]. Available: https://doi.org/10.1007/s10924-016-0837-9.

ISO 527-1, 2012. DIN EN ISO 527-1, Plastics-Determination of Tensile Properties, Part 1: General Principles. International Standard Organization Std.. https://www.iso.org [Online]. Available: https://www.iso.org/fr/standard/56045.html.

ISO 527-2, 2012. DIN EN ISO 527-2, Plastics-Determination of Tensile Properties, Part 2: Test conditions for moulding and extrusion plastics. International Standard Organization Std.. https://www.iso.org [Online]. Available: https://www.iso.org/fr/standard/56046.html.

Johnson, Gordon R., Cook, William H., 1983. A constitutive model and data for metals subjected to large strains, high strain rates and high temperatures. Proceedings of the 7th International Symposium on Ballistics, The Hague, 19-21 April 1983pp. 541–547.

Juliac, E., Arman, J., Harran, D., 1998. Ultrasonic interferences in polymer plates. J. Acoust. Soc. Am. 104 (3), 1232–1241. [Online]. Available: https://doi.org/10.1121/1.424331.

Khan, F., Yeakle, C., Gomaa, S., 2012. Characterization of the mechanical properties of a new grade of ultra high molecular weight polyethylene and modeling with the viscoplasticity based on overstress. J. Mech. Behav. Biomed. Mater. 6, 174–180. Online]. Available: http://www.sciencedirect.com/science/article/pii/S1751616111002736.

Kolarík, J., Pegoretti, A., 2006. Non-linear tensile creep of polypropylene: Time-strain superposition and creep prediction. Polymer 47 (1), 346–356. [Online]. Available: http://www.sciencedirect.com/science/article/pii/S0032386105016460.

Kundu, T. (Ed.), 2013. Ultrasonic and Electromagnetic NDE for Structure and Material Characterization Engineering and Biomedical Applications.

Lagakos, N., Jarzynski, J., Cole, J.H., Bucaro, J.A., 1986. Frequency and temperature dependence of elastic moduli of polymers. J. Appl. Phys. 59 (12), 4017–4031. [Online]. Available: https://doi.org/10.1063/1.336707.

Laperre, J., Thys, W., Lenoir, O., Izbicki, J., 1992. Experimental determination of the transversal wave velocity in plates. J. Acoust. 5, 161–170.

Lefebvre, G., Wunenburger, R., Valier-Brasier, T., 2018. Ultrasonic rheology of viscoelastic materials using shear and longitudinal waves. Appl. Phys. Lett. 112 (24), 241906 [Online]. Available: https://doi.org/10.1063/1.5029905.

Liang, J.-Z., 2012. Predictions of Young's modulus of short inorganic fiber reinforced polymer composites. Compos. Part B 43 (4), 1763–1766. [Online]. Available: http://www.sciencedirect.com/science/article/pii/S1359836812000169.

Madigosky, W.M., Lee, G.F., 1983. Improved resonance technique for materials characterization. J. Acoust. Soc. Am. 73 (4), 1374–1377. [Online]. Available: https://doi.org/10.1121/1.389242.

Martin, N., Mouret, N., Davies, P., Baley, C., 2013. Influence of the degree of retting of

flax fibers on the tensile properties of single fibers and short fiber/polypropylene composites. Ind. Crops Prod. 49, 755–767. [Online]. Available: http://www.sciencedirect.com/science/article/pii/S0926669013003014.

Marrot, L., Bourmaud, A., Bono, P., Baley, C., 2014. Multi-scale study of the adhesion between flax fibers and biobased thermoset matrices. Mater. Des. (1980-2015) 62, 47–56. [Online]. Available: http://www.sciencedirect.com/science/article/pii/S0261306914003628.

Merotte, J., Duigou, A.L., Bourmaud, A., Behlouli, K., Baley, C., 2016. Mechanical and acoustic behaviour of porosity controlled randomly dispersed flax/PP biocomposite. Polym. Test. 51 (Supplement C), 174–180. [Online]. Available: http://www.sciencedirect.com/science/article/pii/S0142941816300174.

Merotte, J., Duigou, A.L., Kervoelen, A., Bourmaud, A., Behlouli, K., Sire, O., Baley, C., 2018. Flax and hemp nonwoven composites: The contribution of interfacial bonding to improving tensile properties. Polym. Test. 66, 303–311. [Online]. Available: http://www.sciencedirect.com/science/article/pii/S0142941817318780.

Mulliken, A., Boyce, M., 2006. Mechanics of the rate-dependent elastic-plastic deformation of glassy polymers from low to high strain rates. Int. J. Solids Struct. 43 (5), 1331–1356. [Online]. Available: http://www.sciencedirect.com/science/article/pii/S0020768305002313.

Mochane, M., Mokhena, T., Mokhothu, T., Mtibe, A., Sadiku, E., Ray, S., Ibrahim, I., Daramola, O., 2019. Recent progress on natural fiber hybrid composites for advanced applications: A review. Exp. Polym. Lett. 13 (2), 159–198. [Online]. Available: http://ww.w.expresspolymlett.com/letolt.php?file=EPL-0009444&mi=c.

Naghmouchi, I., Mutjé, P., Boufi, S., 2015. Olive stones flour as reinforcement in polypropylene composites: A step forward in the valorization of the solid waste from the olive oil industry. Ind. Crops Prod. 72, 183–191. [Online]. Available: http://www.sciencedirect.com/science/article/pii/S0926669014007596.

Nuñez, A.J., Sturm, P.C., Kenny, J.M., Aranguren, M.I., Marcovich, N.E., Reboredo, M.M., 2003. Mechanical characterization of polypropylene-wood flour composites. J. Appl. Polym. Sci. 88 (6), 1420–1428. [Online]. Available: http://dx.doi.org/10.1002/app.11738.

Oksman, K., Nov 2000. Mechanical properties of natural fibre mat reinforced thermoplastic. Appl. Compos. Mater. 7 (5), 403–414. [Online]. Available: https://doi.org/10.1023/A:1026546426764.

Pickering, K., Efendy, M.A., Le, T., 2016. A review of recent developments in natural fibre composites and their mechanical performance. Compos. Part A 83, 98–112. special Issue on Biocomposites. [Online]. Available: http://www.sciencedirect.com/science/article/pii/S1359835X15003115.

Puglia, D., Biagiotti, J., Kenny, J.M., 2005. A review on natural fibre-based composites - Part II. J. Nat. Fibers 1 (3), 23–65. [Online]. Available: https://doi.org/10.1300/J395v01n03_03.

Qiu, K., Netravali, A., 2012. Fabrication and characterization of biodegradable composites based on microfibrillated cellulose and polyvinyl alcohol. Compos. Sci. Technol. 72 (13), 1588–1594. https://doi.org/10.1016/j.compscitech.2012.06.010.

Santoni, A., Bonfiglio, P., Mollica, F., Fausti, P., Pompoli, F., Mazzanti, V., 2018. Vibroacoustic optimisation of Wood Plastic Composite systems. Constr. Build. Mater. 174, 730–740. [Online]. Available: http://www.sciencedirect.com/science/article/pii/S0950061818309590.

Stark, N., 2001. Influence of moisture absorption on mechanical properties of wood flour-polypropylene composites. J. Thermoplast. Compos. Mater. 14 (5), 421–432. [Online]. Available: https://doi.org/10.1106/UDKY-0403-626E-1H4P.

Scalerandi, M., Gliozzi, A.S., Bruno, C.L.E., Antonaci, P., 2012. Nonequilibrium phenomena in damaged media and their effects on the elastic properties. J. Acoust. Soc. Am. 131 (6), 4304–4315. [Online]. Available: https://doi.org/10.1121/1.4707529.

Schiavi, A., Prato, A., 2017. Evidences of non-linear short-term stress relaxation in polymers. Polym. Test. 59, 220–229. [Online]. Available: http://www.sciencedirect.com/science/article/pii/S0142941816312168.

Simonetti, F., Cawley, P., 2004. Ultrasonic interferometry for the measurement of shear velocity and attenuation in viscoelastic solids. J. Acoust. Soc. Am. 115 (1), 157–164. [Online]. Available: https://doi.org/10.1121/1.1631944.

Simonetti, F., Cawley, P., DemÄ enko, A., 2005. On the measurement of the youngâ€™s modulus of small samples by acoustic interferometry. J. Acoust. Soc. Am. 118 (2), 832–840. [Online]. Available: https://doi.org/10.1121/1.1942387.

Siviour, C.R., Jordan, J.L., Mar 2016. High strain rate mechanics of polymers: A review. J. Dyn. Behav. Mater. 2 (1), 15–32. [Online]. Available: https://doi.org/10.1007/s40870-016-0052-8.

Swolfs, Y., Verpoest, I., Gorbatikh, L., 2019. Recent advances in fibre-hybrid composites: materials selection, opportunities and applications. Int. Mater. Rev. 64 (4), 181–215. [Online]. Available: https://doi.org/10.1080/09506608.2018.1467365.

Tanguy, M., Bourmaud, A., Beaugrand, J., Gaudry, T., Baley, C., 2018. Polypropylene reinforcement with flax or jute fibre; influence of microstructure and constituents properties on the performance of composite. Compos. Part B 139, 64–74. [Online]. Available: http://www.sciencedirect.com/science/article/pii/S1359836816328438.

Tausif, M., Pliakas, A., O'Haire, T., Goswami, P., Russell, S.J., 2017. Mechanical properties of nonwoven reinforced thermoplastic polyurethane composites. Materials 10 (6), 618–631. [Online]. Available: http://www.mdpi.com/1996-1944/10/6/618.

Waterman, H.A., 1963. Determination of the complex moduli of viscoelastic materials with the ultrasonic pulse method (Part I). Kolloid-Z. Z. Polym. 192 (1), 1–8. [Online]. Available: https://doi.org/10.1007/BF01499756.

Zihlif, A.M., Duckett, R.A., Ward, I.M., Apr 1982. The determination of the lateral compliances and Poisson's ratios for highly oriented polyethylene sheets. J. Mater. Sci. 17 (4), 1125–1130. [Online]. Available: https://doi.org/10.1007/BF00543532.